

LM-00K013
February 22, 2000

Thermodynamic Analysis of Thermophotovoltaic Efficiency and Power Density Tradeoffs

P.F. Baldasara, J.E. Reynolds, G.W. Charache, D.M. DePoy, C.T. Ballinger,
T. Donovan, J.M. Borrego

NOTICE

This report was prepared as an account of work sponsored by the United States Government. Neither the United States, nor the United States Department of Energy, nor any of their employees, nor any of their contractors, subcontractors, or their employees, makes any warranty, express or implied, or assumes any legal liability or responsibility for the accuracy, completeness or usefulness of any information, apparatus, product or process disclosed, or represents that its use would not infringe privately owned rights.

Thermodynamic Analysis of Thermophotovoltaic Efficiency and Power Density Tradeoffs

P.F. Baldasaro, J.E. Reynolds, G.W. Charache, D.M. DePoy, C.T. Ballinger, and T. Donovan

Lockheed Martin Inc., Schenectady, NY 12301-1072

J. M. Borrego

Department of Electrical, Computer, and Systems Engineering
Rensselaer Polytechnic Institute, Troy, NY 12180-3590

ABSTRACT

This report presents an assessment of the efficiency and power density limitations of thermophotovoltaic (TPV) energy conversion systems for both ideal (radiative-limited) and practical (defect-limited) systems. Thermodynamics is integrated into the unique process physics of TPV conversion, and used to define the intrinsic tradeoff between power density and efficiency. The results of the analysis reveal that the selection of diode bandgap sets a limit on achievable efficiency well below the traditional Carnot level. In addition it is shown that filter performance dominates diode performance in any practical TPV system and determines the optimum bandgap for a given radiator temperature. It is demonstrated that for a given radiator temperature, lower bandgap diodes enable both higher efficiency and power density when spectral control limitations are included. The goal of this work is to provide a better understanding of the basic system limitations that will enable successful long-term development of TPV energy conversion technology.

I. INTRODUCTION

There is currently a resurgence of development activity in the area of thermophotovoltaic (TPV) energy conversion that has been driven by the advancements in III-V semiconductor technology and the potential use of TPV in a wide range of applications. TPV systems have several performance advantages over other heat conversion systems, including: 1) the wide range of available fuel sources provides versatility, 2) the absence of moving parts provides low noise and high reliability, and 3) the ability to recover waste heat provides a potentially higher system efficiency ($> 20\%$). The challenge in the development of TPV systems is to achieve acceptable efficiency and power density within reasonable hot-side temperature limits ($T_h < 1500\text{ }^\circ\text{C}$).

There have been a number of attempts to quantify the performance limits of TPV energy conversion [1-6]. Most studies focus solely on the thermodynamic limits of the energy conversion diode, and are based on the approach of Shockley and Quieser [7] which assumes perfect or no spectral control and neglect cavity effects. Woolf, in contrast, was the first to quantify the dramatic impact of non-ideal spectral control on efficiency [4]. This paper expands on these earlier works and attempts to quantify the limits of TPV performance from an integral system viewpoint, including: 1) photonic angular dispersive effects of the radiator and filter, 2) the sensitivity of system efficiency, power density, voltage factor and fill factor to the bandgap of the diode, 3) the sensitivity of system efficiency and power density to close-spaced radiator and high injection level effects, and 4) the sensitivity of system efficiency to the integration of the radiator, spectral control, diode and cavity components.

A TPV system is an example of a photonic heat engine. Therefore, the system is subject to thermodynamic (entropy generation) limitations where the maximum efficiency (η_{Carnot}) is bounded by the operating temperature limits of the heat source (T_h) and the heat sink (T_c) (i.e., $\eta_{\text{Carnot}} = (T_h -$

T_c/T_h). The Carnot formulation is misleading in that it implicitly assumes the absence of internal entropy sources, (i.e., irreversible losses). However, in a real heat engine where work is performed, internal entropy sources must be considered in the determination of achievable efficiency. The entropy sources in a TPV system include the following efficiency losses: 1) temperature drops necessary to transport heat from the heat source to the blackbody radiator, 2) electric current flow necessary to generate power, and 3) illumination-induced deviations from diode equilibrium.

The basic components of a TPV conversion system are described in Figure 1 and include: a blackbody photon radiator, a photon spectral control device (i.e., filter) to minimize parasitic photon absorption, and a voltaic diode with a bandgap, E_g , to convert blackbody radiation into electric power. This report quantifies the role of each component (i.e., radiator, filter, and diode) from a photonic heat engine viewpoint and presents an assessment of TPV system performance issues related to the integration of the components.

II. RADIATOR CONSIDERATIONS

The TPV conversion process begins with the emission of energy from a radiator assumed to be a Lambertian surface. This source has the frequency and angular characteristics of energy radiated from a small hole in a blackbody cavity. The standard derivation of thermal radiator blackbody emission proceeds by calculating the energy density (energy/volume) of equilibrium photons at a temperature, T_h [8]. The total energy density, ρ_E , is given as the integral of the phase-space volume, $[2/(2\pi\hbar)^3] \cdot d^3r \cdot d^3\vec{p}$, times the Bose-Einstein occupation probability, $f(\omega, T_h)$, times the energy per photon, $\hbar\omega$, where \vec{p} is momentum and r is position. Using $p = \hbar\vec{k}$, where the wavevector $|\vec{k}| = \omega/c$, the total energy density is given by:

$$\rho_E = \frac{\hbar}{4\pi^3 c^3} \cdot \int \omega^3 f(\omega, T_h) \sin \theta \cdot d\omega \cdot d\theta \cdot d\varphi \equiv \int \rho_E(\omega, \theta, \varphi) \cdot d\omega \cdot d\Omega, \quad (1)$$

where, ω is the frequency, c is the speed of light, \hbar is Planck's constant divided by 2π , θ is the polar angle, φ is the azimuthal angle and $d\Omega = \sin\theta \cdot d\theta \cdot d\varphi$. The Poynting vector (energy current density), $\vec{P}(\omega, \theta, \varphi)$, is given by $c \cdot \vec{s} \cdot \rho_E(\omega, \theta, \varphi)$, where \vec{s} is the photon direction. The intensity of radiation, $I(\omega, \theta, \varphi)$, emitted from a blackbody is obtained by taking the dot product of the Poynting vector and the unit normal, \vec{n} :

$$I(\omega, \theta, \varphi) \cdot d\omega \cdot d\Omega = \vec{P}(\omega, \theta, \varphi) \cdot \vec{n} \cdot d\omega \cdot d\Omega = \frac{\hbar}{4\pi^3 c^2} \cdot \omega^3 \cdot f(\omega, T_h) \cdot \cos \theta \cdot d\omega \cdot d\Omega \quad (2)$$

Integrating EQ 2 over a hemispherical (forward) solid angle yields the frequency dependent energy emission rate:

$$I(\omega) = \frac{\hbar \omega^3}{4\pi^2 c^2} \cdot \left[\exp\left(\frac{\hbar \omega}{k_B T_h}\right) - 1 \right]^{-1} \quad (3)$$

where, k_B is Boltzmann's constant. Integrating EQ (3) over frequency yields the well-known Stefan-Boltzmann surface radiation equation, $I = \sigma T_h^4$, where $\sigma = \pi^2 k_B^4 / 60 \hbar^3 c^2$ is the Stephan-Boltzmann constant.

A. FREQUENCY DISPERSION

It is convenient to compare blackbody radiators in the TPV range of interest (1000 °C - 1500 °C) to the more familiar solar source. Figure 2 compares the frequency dispersion of the energy density for solar radiation incident at the Earth's surface (~6000 °C) and blackbody radiation at the TPV radiator surface (~1000 °C). The TPV blackbody source shows a significantly lower average frequency content (i.e., longer average wavelength) at the lower temperature (1000 °C vs. 6000 °C).

Lower average frequency is analytically correlated to lower temperature via Wien's law which defines the most probable frequency of the blackbody spectrum as being proportional to radiator temperature: $T_b / \omega_{\max} = 1.54 \times 10^{-12}$ sec-K. Higher average frequency (i.e., energy) content also scales with ω_{\max} , which indicates that lower temperature sources have lower frequency (i.e., energy) content.

B. ANGULAR DISPERSION

A TPV filter must accommodate photons at all incident angles from 0-90°. As shown in EQ (2), the angular dispersion of photons emitted from a Lambertian TPV radiator surface has a $\sin\theta \cdot \cos\theta$ dependence. The TPV radiator angular dispersion has a peak at 45°, quite unlike solar radiation incident on the Earth, having near-normal angle because of the Earth-sun separation. The large angular dispersion of a radiative blackbody thermal photon source in TPV conversion complicates filter design and performance as discussed in Section III.B below.

C. PHOTON EMISSION RATE

Blackbody radiation emission rates are well known, as established in EQ (1). The Stefan-Boltzmann equation however, does not represent the maximum limit of photon emission rate from a surface. The EQ (1) blackbody derivation makes the assumption that the spatial separation, d , between the radiator and the receiver is much greater than the wavelength of the emitted photons. In the more general case where d may be comparable to the photon wavelength, the energy transfer between two surfaces is a function of their dielectric properties [9 -13]. This is because the radiator/receiver dielectric function contains the material-dependent photon density-of-states information. In effect, the traditional blackbody radiator case limits the photon density-of-states to that of free space, which

represents a lower density-of-states limit. The only thermodynamic criterion involved in thermal emission from a surface is represented by the state occupation number, $N(\omega)$.

References 11-13 provide an assessment of the effects of surface spacing and temperature on photon emission for the more general, and much more complicated close-spaced case. Figure 3 shows that close-spacing offers the potential for much higher ($\sim 10\times$) energy transfer rates [11]. Because the radiator/receiver dielectric functions are not thermodynamically bounded, their optimum selection could have major impact on the efficiency/power density tradeoff, as well as filter and diode parameter selection.

III. FREQUENCY SPECTRUM CONTROL CONSIDERATIONS

The TPV process can be conceptualized as the selective conversion of the photons from a blackbody radiator which have energies greater than the bandgap (E_g) of the TPV diode. The process is enabled by a filter that reflects photons of unusable energy ($< E_g$) back to the radiator. In essence, a filter is a photon recuperator that returns low-quality energy back to the radiator for reabsorption. Thus, less energy from a heat source is required to keep the radiator at the same temperature. Although filter reflectivity (recuperation) has no thermodynamic limit, it plays a key part in the overall system efficiency. As a result of the unique frequency and angular dispersion attributes of blackbody radiation, the issues associated with spectral control of TPV blackbody radiation are significantly different for solar radiation.

The most general approach to the spectral control design process is to solve Maxwell's Equations in three spatial dimensions with an "appropriately" chosen dielectric function, $\epsilon(r,\omega)$, and conductivity, $\sigma(r,\omega)$. Both ϵ and σ are generally functions of position, r , and frequency, ω and are

selected to maximize above-bandgap energy current while minimizing below-bandgap energy current. Both $\epsilon(r,\omega)$ and $\sigma(r,\omega)$ are material dependent via molecular and/or electronic polarizability. From a design space viewpoint, $\epsilon(r,\omega)$ and $\sigma(r,\omega)$ can be varied either by materials selection or spatial distribution. The filter design process then conceptually reduces to the determination of the optimum compositional and/or dimensional variation of $\epsilon(r,\omega)$ and $\sigma(r,\omega)$ with respect to the frequency and angular dispersion attributes of blackbody radiation.

A. FREQUENCY DISPERSION

A key issue with spectral control in TPV conversion is the low fraction of usable energy ($E > E_g$) in the radiated blackbody spectrum. Figure 4 shows the fraction of usable above-bandgap energy versus bandgap for a radiator temperature of 1000 °C. For example with $E_g > 0.5$ eV, the usable energy fraction is less than 30%. Therefore, efficient TPV applications require filters with very high reflectivities for energies below the bandgap, and very-high transmissivities for energies above the bandgap. The large frequency dispersion of a blackbody radiator requires a wide filter reflection bandwidth (2-12 μm). This impacts above bandgap transmission because of harmonic reflection bands, and harmonic suppression techniques must be utilized when designing a filter over the entire blackbody frequency spectrum.

Although filter efficiency (reflection and transmission) can in theory be 100%, the presence of absorption anywhere in the filter introduces irreversible losses and lowers filter efficiency. Again, the large frequency dispersion of a blackbody radiator restricts materials options because of absorption processes in real materials. In addition, the low fraction of usable above-bandgap energy amplifies the effect of parasitic absorption.

B. ANGULAR DISPERSION

The high angular dispersion of TPV blackbody radiation complicates the use of dimensional control (interference processes) in three ways:

- Interference depends on optical thickness of filter layers, which in turn depends on the angle of photon incidence. A fixed spatial design therefore causes a filter efficiency compromise with a 0° - 90° angular dispersion.
- High angular dispersion of incident photons and non-specular reflections within the energy conversion device leads to the potential for optical frustration [14], (i.e. high refraction index trapping and multiple internal reflections within the diode/filter). Frustration can be a major parasitic absorption loss process even for low absorption systems because of the long integral transport path caused by multiple reflections.
- High angle scattering limits absorption of useful above-bandgap photon energy. At high incidence angles of greater than 70° , which represent $\sim 12\%$ of the TPV blackbody photon population, the reflection probability increases, as predicted from Fresnel's laws ($R \propto \sin^2 \theta$). High angle reflection limits the integral absorption of useful above-bandgap energy.

C. PHOTON EMISSION RATE

The more general case of a close-spaced radiator ($d \leq \lambda$) also impacts filter design and performance. In the close-spaced configuration we must abandon the concept of a photon traveling through space from radiator to diode, and think instead of energy transfer via radiator/diode dielectric coupling across a fractional wavelength gap. This alters the notion of spectral control from being a filter characteristic, to being a "system" characteristic of the radiator/filter/diode dielectric materials

selection. In essence, it becomes necessary to "tune" the radiator dielectric to the diode interband transition. The close-spaced concept opens new avenues for frequency selectivity and opportunities for increased power density [11-13].

IV. VOLTAIC DIODE CONSIDERATIONS

A. BANDGAP CONSIDERATIONS

Assessment of diode thermodynamic performance limits is complicated by the multiple processes involved in voltaic conversion, which each have a unique dependence on diode bandgap. Figure 5 presents the voltaic conversion process in energy diagram format, assuming a p/n polarity with all photon absorption in the p-type emitter. The TPV conversion process proceeds with the absorption of an arbitrary photon of energy $E = E_g + \Delta E_o$, and the creation of a mobile electron/hole pair, where ΔE_o is the excess energy above the bandgap. Carrier collection (current generation) occurs at the p/n interface, as the built-in electric field separates electrons from holes (eg. electrons accelerated into the n-type region). Illumination-induced diode current produces an operating voltage which enables transmission of power to a load. For analytic purposes the TPV conversion process is differentiated into four sub-processes [15,16]: (1) photon absorption/current generation or quantum efficiency (QE), (2) photon overexcitation efficiency (F_o), (3) open circuit voltage efficiency (V_{oc} / E_g), and (4) power usage efficiency or fill factor (FF). Diode efficiency is the product of these four processes:

$$\eta_{diode} = QE \cdot F_o \cdot V_{oc} / E_g \cdot FF \quad (4)$$

Differentiation of current and voltage generation into four sub-processes is arbitrary, but conforms to existing solar photovoltaic nomenclature and allows each process to be evaluated independently.

1. QUANTUM EFFICIENCY

Quantum efficiency (QE) is determined by the diffusion length and surface recombination velocity of semiconductor materials. It is possible in theory to achieve diffusion lengths many times the diode thickness and obtain QE of 1.0 (excluding the occurrence of impact ionization where the QE may be greater than 1.0). QE ~ 1.0 has in fact been demonstrated in well developed solar photovoltaic applications and in some TPV systems [16]. The TPV process is not thermodynamically limited by QE, and henceforth is assumed to be 1.0.

2. PHOTON OVEREXCITATION EFFICIENCY

The photon overexcitation efficiency (F_o) represents irreversible losses associated with excited carrier relaxation. Photon absorption requires that the photon energy must be $> E_g$ by an amount ΔE_o . The excess energy degrades rapidly because the high density of energy states above E_g leads to rapid ($\sim 10^{-13}$ sec) energy relaxation until the carrier reaches the bandgap energy, which represents a metastable energy level ($\sim 10^{-8}$ sec) because of the energy gap. This relaxation (heat generation) process is irreversible, and leads to an intrinsic efficiency loss. F_o is defined, as the fraction of absorbed above-bandgap photon energy that is usable, (i.e., not lost to overheating):

$$F_o = \frac{\frac{E_g}{\hbar} \int_{E_g/\hbar}^{\infty} \frac{\omega^2}{2\pi^2 c^2} \left(\exp\left(\frac{\hbar\omega}{k_B T_h}\right) - 1 \right)^{-1} d\omega}{\int_{E_g/\hbar}^{\infty} \frac{\omega^3}{2\pi^2 c^2} \left(\exp\left(\frac{\hbar\omega}{k_B T_h}\right) - 1 \right)^{-1} d\omega} \quad (5)$$

F_o increases as E_g increases for a given blackbody radiator temperature, because a smaller fraction of the photonic energy is $> E_g$. Figure 6 shows a plot of F_o vs E_g for a blackbody radiator temperature of

1000 °C.

3. VOLTAGE GENERATION

To understand voltage generation (V_{oc} / E_g), the electrochemical nature of the voltaic conversion process must be recognized. In the "unilluminated" (i.e. dark) condition, the high chemical potential built into the diode via the p and/or n impurity doping concentrations ($\sim 10^{18} \text{ cm}^{-3}$) on either side of the p/n junction interface is cancelled by an electric potential which develops from carrier migration across the junction. This balance is characterized as electrochemical equilibrium in the "unilluminated" condition. This equilibrium is disturbed by illumination, as mobile minority carriers diffuse to the junction, and are accelerated by the built-in electric field. The transformation of minority carriers into majority carriers at the junction interface alters the equilibrium condition, and creates an electrochemical potential gradient that is manifested as a measured output voltage.

The thermodynamic limit on voltage generation is not intuitively obvious, but can be inferred from Figure 5 and the diode equation in the open circuit condition:

$$J_{net} = -J_{sc} + J_r [\exp(V_{oc} / k_B T) - 1] = 0 \quad (6a)$$

$$V_{oc} = k_B T_c \ln(J_{sc}/J_r + 1), \quad (6b)$$

where, T_c is the cold-side/diode temperature, J_{sc} is the short circuit current density, and J_r is the dark current density in the unilluminated condition. EQ (6b) indicates that the J_{sc}/J_r ratio determines voltage generation. With J_{sc} intuitively limited by the blackbody radiator temperature (photon flux), this implies that there must be a thermodynamic limit on J_r . In the general case, J_r has contributions from several sources including: Shockley-Read Hall (SRH), Auger, and radiative recombination processes [16].

While SRH and Auger processes can in theory be negligible, there is a definite limit J_r from radiative recombination, which is set by the unilluminated equilibrium blackbody radiation emanating from the diode surface at temperature T_c . This recombination rate can be calculated by integrating the blackbody spectrum over the full range of photon frequencies from the bandgap frequency to infinity in the unilluminated ($V = 0$) case [17]. The result is given by:

$$J_r = \frac{q(n^2 + 1)}{4\pi^2 c^2} \int_{E_g/\hbar}^{\infty} \omega^2 \exp\left[\frac{\hbar\omega}{k_B T_c} - 1\right]^{-1} d\omega \cong \frac{q(n^2 + 1)}{4\pi^2 c^2 \hbar^3} \exp[-E_g/kT_c] \cdot \left[E_g^2 kT_c - 2(kT_c)^3 \left[\frac{E_g}{k_B T_c} - 1 \right] \right]. \quad (7)$$

When $E_g \gg kT_c$, the -1 in the exponential of the integral of Eq. 7, and the T_c^3 term on the right hand side, can be neglected to give $J_r = q(n^2 + 1)E_g^2 kT_c (4\pi^2 \hbar^3 c^2)^{-1} \exp(-E_g/kT_c)$, where q is the electronic charge, and n is the diode index of refraction. When a back surface reflector is added to the diode, the term $n^2 + 1$ is replaced by 1, thus reducing the radiative dark current as a result of photon recycling [16,17]. EQ (7) defines the thermodynamic (temperature-based) limit on J_r . It is interesting to note that J_r in EQ (7) has the same exponential dependence on bandgap as the more traditional drift-diffusion formulation [18], both of which are a consequence of detailed balance. J_{sc} can be obtained analytically in the same manner as J_r , recognizing that the blackbody radiation characteristic has the same functionality as J_r , because it is derived from the same blackbody integral as in EQ (7), but with the temperature elevated to T_h , again assuming $E_g \ll k_B T_h$. Therefore:

$$J_{sc} = \frac{q(n^2 + 1)}{4\pi^2 c^2 \hbar^3} T_h \exp[-E_g/k_B T_h]. \quad (8)$$

The dependence of V_{oc} with bandgap can then be evaluated by substituting EQ's (7) and (8) into (6), and noting that $J_{sc}/J_r \gg 1$:

$$\frac{V_{oc}}{E_g} = 1 - \frac{T_c}{T_h} + \frac{k_B T_c}{E_g} \ln \left[\frac{T_h}{T_c} \right]. \quad (9)$$

EQ (9) indicates that the thermodynamic open circuit voltage factor (V_{oc} / E_g) approximates (but is actually higher than) the Carnot efficiency by a factor $\sim k_B T_c / E_g$. Figure 6 shows the unexpected result of increasing open circuit voltage factor with decreasing bandgap for $T_h = 1000$ °C and $T_c = 25$ °C. The mechanistic explanation of this functionality lies in the electrostatic potential at the diode junction (see Figure 5). In the open circuit condition, the illumination-induced injection current and the voltage-induced reverse current all recombine at the diode junction. These recombination processes reduce the junction electric field, which is the source of the electrostatic potential across the junction in the first place. A lower junction electric field leads to a higher open circuit voltage, and lower bandgap leads to higher current recombination and subsequently to higher V_{oc} / E_g .

4. FILL FACTOR

The fill factor is defined as the maximum diode output power density ($P_m = V_m J_m$) divided by $J_{sc} V_{oc}$, where V_m and J_m are the voltage and current density, respectively at P_m . The fill factor represents the maximum power density between the two extremes of short circuit current ($V = 0$), and open circuit voltage ($J = 0$), and quantifies the ability of the TPV diode to deliver power to the load.

Fill factor performance also has an electrochemical interpretation. In Figure 5, qV_m represents the free energy of the voltaic process or the separation of the quasi-Fermi levels, (i.e., that fraction of the bandgap energy that is available to do useful work) while qV_s represents an irreversible energy loss (entropy creation) process from charge acceleration across the junction electric field. On crossing the junction, potential energy is transformed into kinetic energy. This excess kinetic energy is transformed

into heat as carriers relax to the potential energy minimum on the other side of the junction. Recognizing qV_m as the available free energy from the photon absorption process, leads to the following relationship:

$$qV_m = E_g - qV_s = E_g - T_c S. \quad (10)$$

Hence, $qV_s = T_c S$, defines qV_s / T_c as an entropy source term in the TPV conversion process. Note, for simplicity it is assumed that the doping level of the diode is sufficiently high such that the separation of the n- and p-quasi-Fermi level's from the conduction and valence-bands, respectively are negligible. The heat generation process associated with V_s can also be recognized also as Peltier heat, and is conceptually identical to the heat rejection process in thermoelectric conversion. Likewise, qV_s / T_c (the entropy creation term) is proportional to the Seebeck coefficient of the voltaic p/n junction. Interestingly, the same junction electrostatic potential that enables voltage generation also causes process irreversibility.

An explicit expression for the fill factor in terms of V_m can be derived using the ideal diode equation assuming zero series and infinite shunt resistance, and maximizing the power with respect to voltage, giving the standard expressions for V_m and J_m [18]:

$$J_m = J_{sc} / (1 + k_B T_c / qV_m) \sim J_{sc} (1 - k_B T_c / qV_m), \text{ and} \quad (11)$$

$$V_m = V_{oc} - \frac{k_B T_c}{q} \ln \left[\frac{qV_m}{k_B T_c} \right]. \quad (12)$$

Rearranging EQ's 10 and 11 yields the fill factor:

$$FF = \frac{J_m V_m}{J_{sc} V_{oc}} = \frac{V_m - k_B T_c / q}{V_m + \frac{k_B T_c}{q} \ln \left[\frac{qV_m}{k_B T_c} \right]} \quad (13)$$

Noting that V_m (like V_{oc}) is solely a function of the J_{sc}/J_r ratio, identifies V_m , and subsequently the fill factor, as a thermodynamic function of J_{sc}/J_r . EQ's (13) and EQ (9) together permit analytic determination of V_m as a function of E_g . As seen in Figure 6, the fill factor is an increasing function of bandgap with maximum value of 1 (Again, this figure assumes $T_h = 1000$ °C, $T_c = 25$ °C). The mechanistic explanation of the fill factor functionality lies in the recognition of the Peltier heat as an entropy generation (irreversible) process. As bandgap is lowered, higher J_{sc} leads to increased entropy generation per unit work. In practical systems, finite series and shunt resistances will also degrade fill factor from these ideal values. These additional loss mechanisms increase in significance as bandgap decreases or radiator temperature increases due to increased J_{sc} .

EQ (11) indicates that the reverse current at the maximum power point is $J_{sc}k_B T_c / qV_m$. This reverse current must appear as radiative emission because of the assumption of carrier radiative recombination. Therefore, a correction must be made to EQ(4) to account for the reduction in the net heat absorbed by the amount $J_{sc}k_B T_c E_g / qV_m$. The efficiency correction factor is given as:

$$F_r = \frac{\frac{J_{sc} E_g}{F_o} - \frac{J_{sc} E_g k_B T_c}{qV_m}}{\frac{J_{sc} E_g}{F_o}} = 1 - \frac{F_o k_B T_c}{qV_m} \quad (14)$$

5. EFFICIENCY/POWER DENSITY TRADEOFF

The results presented above define an intrinsic thermodynamic tradeoff between power density and efficiency as a function of bandgap. Figure 7 quantifies this tradeoff for two cases: 1) a thermodynamically-limited (i.e., zero defect, photon-recycled) TPV diode, and 2) for a 100x increase in J_r over a thermodynamically-limited diode. Both cases assume a perfect filter. Note that as bandgap

increases, power density approaches zero, and efficiency approaches the Carnot limit ($T_h = 1000$ °C, $T_c = 25$ °C, $\eta_{\text{Carnot}} = 75\%$), consistent with the Carnot criterion of zero irreversibility and zero work capability.

B. HIGH CURRENT INJECTION EFFECTS

The analysis in the previous sections defined the thermodynamic-limit (i.e., zero defect, photon-recycled) on dark current in low-level injection. Although there are several practical difficulties (eg. SRH and Auger recombination) in achieving such high performance, it has been approached in various III-V laser and photovoltaic systems. It is then reasonable to question what other effects exist to prevent attainment of perfect diode performance. In this regard, the effects of high-level injection (i.e. high illumination levels) on efficiency are discussed in this section.

As a conceptual exercise, consider a close-spaced radiator configuration where the radiator dielectric constant is n^2 (i.e. case of electrically insulating radiator). In this simplified case, the photon density-of-states increases in proportion to n^3 and the subsequent photon flux increases in proportion to n^2 over a classical blackbody radiator. In order to quantify the effect of the n^2 increase in photon flux and the effect of illumination level on the J_{sc}/J_r ratio, the density-of-states term is modified in the derivation of J_r in EQ (7). This yields, J_r (close-spaced) = $n^2 J_r$ (blackbody), (i.e., thermal equilibrium mandates the same density of states dependence of J_{sc} and J_r , which differ only in their respective temperatures). Therefore, the equilibrium J_{sc}/J_r ratio and dependent thermodynamic parameters (i.e., V_{oc}/E_g and FF) do not theoretically change as a result of the increased close-spacing energy exchange.

Now consider the effects of non-equilibrium conditions, noting that the basic expressions for J_r

and J_{sc} in Eqn's (7) and (8) were derived with an equilibrium assumption (i.e., low-level injection). This equilibrium assumption is always approximate in that the photon absorption and electron excitation always increases the "effective electron temperature". (The limit of this electron temperature perturbation is represented by population inversion where the effective electron temperature actually exceeds that of the illuminating source.) It is clear that J_r will increase as the light injection level and effective electron temperature increase.

As an approximation, one may consider a "significant" equilibrium perturbation to occur when the semiconductor doping level (N_a) no longer determines the minority carrier concentration (i.e., $\Delta n > N_a$). The J_{sc} limit (J_{lim}) for high injection can be estimated from the open circuit condition, where illumination and reverse injection currents are equal:

$$J_{lim} = qW N_a / \tau_{lim}, \quad (15)$$

Where, W is the device thickness, and τ_{lim} is the net minority carrier lifetime. EQ (15) indicates that the high injection condition is enabled by high carrier lifetime, and that as diode quality improves and lifetimes approach the radiative limit, the high injection condition is more likely. For typical doping levels of 10^{17} cm^{-3} , minority carrier lifetimes of 500 ns, and device thickness of 5 μm , EQ (15) yields a value of $\sim 16 \text{ A/cm}^2$ for J_{lim} .

V TPV SYSTEM INTEGRATION CONSIDERATIONS

A. FILTER / DIODE COUPLING

The diode discussion in Section IV was based on the assumption of a perfect filter, i.e. no parasitic photon absorption for energy $< E_g$. Given the low fraction of usable energy, and high frequency and angle dispersion of blackbody radiation, together with the limitations of available filter

materials, less than perfect reflectivity (i.e., zero parasitic absorption) will be achieved for below-bandgap energy in any real application. The impact of less than perfect spectral control on TPV conversion efficiency, and the dependent relationship between diode and filter development are discussed in this section.

As noted in Section III, bandgap selection determines the fraction of usable energy for a given radiator temperature, thereby affecting filter performance. The spectral efficiency (η_{spectral}) is defined as the fraction of total absorbed radiation with energy greater than the bandgap:

$$\eta_{\text{spectral}} = \frac{\int_{E_g/h}^{\infty} \int_0^{\pi/2} \int_0^{\pi} [1 - R(\omega, \theta, \varphi) - \alpha(\omega, \theta, \varphi)] I(\omega, \theta, \varphi) d\omega d\theta d\varphi}{\int_0^{\infty} \int_0^{\pi/2} \int_0^{\pi} [1 - R(\omega, \theta, \varphi)] I(\omega, \theta, \varphi) d\omega d\theta d\varphi} \quad (16)$$

where $R(\omega, \theta, \varphi)$ is the angle and frequency dependent filter reflectivity, $\alpha(\omega, \theta, \varphi)$ is the angle and frequency dependent filter absorptivity of a front surface filter, and $I(\omega, \theta, \varphi)$ is the angle and frequency dependent incident energy flux spectrum given by EQ 2. Figure 8 presents calculations of overall TPV efficiency $\eta = \eta_{\text{diode}} \eta_{\text{spectral}}$, in which the filter and diode performance are integrated as a function of bandgap and filter reflectivity. Here, ideal diode performance is assumed, and filter reflectivity is assumed to be a constant value versus wavelength below bandgap.

Figure 8 shows that even low parasitic absorption levels ($R < 99\%$) have a significant degrading effect on system efficiency, which is counter to the Section IV conclusion that higher bandgap always yields higher efficiency. Figure 8 also reveals the very important result that filter performance (recuperation) in TPV systems is dominant over diode performance (conversion), and in effect determines the optimum diode bandgap.

The strong efficiency dependence on filter performance is a result of the relatively low fraction

of above bandgap photons as initially noted in Section II. Because only a fraction of the total spectrum is usable, recuperation plays a dominant role in the thermodynamic heat conversion cycle. It is a key conclusion that lower bandgap diodes enable **both** higher power density **and** higher efficiency when spectral control limitations are included.

B. CAVITY DESIGN ISSUES

Real TPV system applications often introduce unique photon processes which affect efficiency and power density. For example, a TPV converter must necessarily involve some sort of cavity [Fig. 9] [19]. From a photonic viewpoint, the key cavity attributes are: 1) non-active diode areas, which represent parasitic absorption sites, 2) angular dependent radiator emissivity (i.e., non-Lambertian), which cause multiple reflections and alter the cavity angular dispersion, 3) angular and polarization dependent filter reflectivity, 4) finite separation between radiator and diode which alters the angular dispersion, and 5) cavity edge leakage.

These non-ideal attributes greatly complicate the photon recuperation process and filter design. As an example, Figure 10 shows a Monte Carlo analysis of the Fig. 9 cavity, where the reflectivity of internal structures (cavity walls, diode busbars) is varied. In Figure 10, a module efficiency factor, η_M is included to quantify the effects of parasitic non-active diode area photon absorption. The factor η_M is defined as the total photonic energy absorbed in active diode area divided by total photonic energy absorption. Even for low absorption fraction of $< 10\%$, there is a significant degradation in overall efficiency. This is the result of multiple reflections of below-bandgap photons, which eventually find a parasitic removal site from the system. Again, the spectral control process dominates system performance and must therefore be viewed in terms of the cavity and not just the diode.

VI. CONCLUSIONS

This report defines the functional tradeoff between TPV system efficiency and power density. This tradeoff is a consequence of unavoidable internal entropy generation introduced by the conversion process, which increases as the work rate (current) increases. The identification and quantification of specific TPV process physics limitations shows the need for integrated TPV system component development. The key technical points are repeated in the summary below:

- 1) Filter performance dominates diode performance in a TPV system and determines the optimum bandgap for a given radiator temperature.
- 2) Low bandgap diodes are conceptually enabling for both higher TPV efficiency and higher power density when spectral control limitations are included.
- 3) There is a thermodynamic tradeoff between efficiency and power density, which limits achievable efficiency well below the theoretical Carnot level.
- 4) Classical blackbody radiation does not represent the limit for TPV power density. The more general case of a close-spaced radiator/diode offers a superior efficiency/power density characteristic.
- 5) Radiator, filter, and diode technology must be developed from a system perspective.

REFERENCES

- [1] J.R. Yeargan, R.G. Cook, and F.W. Sexton, Proc. 12th IEEE Photovoltaic Specialists Conference, 807, (1981).
- [2] F. Demichelis, E. Minetti-Mezzetti, M. Agnello, and E. Tresso, J. Appl. Phys., **53**, 9098 (1982).
- [3] J.L. Duomarco, and R. Kaplow, Solar Energy, **32**, 33 (1984).
- [4] L.D. Woolf, Solar Cells, **19**, 19 (1986).
- [5] J.L. Gray, and A. El-Husseini, Proc. 2nd NREL Conf. on Thermophotovoltaic Generation of Electricity, AIP Conf. Proc. **358**, 3 (1996).
- [6] G.D. Cody, Proc. 4th NREL Conf. on Thermophotovoltaic Generation of Electricity, AIP Conf. Proc. **460**, 58 (1999).
- [7] W. Shockley and H.A. Queisser, J. Appl. Phys., **32**, 510 (1961).
- [8] M. Planck, Verh. D. Deut. Physik. Gesell., **2**, 237 (1900).
- [9] M. Levin, V.G. Polevoi, and S. Rytov, "Contribution to the Theory of Heat Exchange Due to a Fluctuating Electromagnetic Field," Sov. Phys. JETP, **52**, 1054 (1980).
- [10] D. Polder and M. Van Hove, "Theory of Radiative Heat Transfer Between Closely Spaced Bodies," Phys. Rev. B, **4**, 3303 (1971).
- [11] J.E. Reynolds, "Enhanced Electromagnetic Energy Transfer Between a Hot and Cold Body at Close Spacing due to Evanescent Fields," AIP Conf. Proc. **460**, 49 (1999).
- [12] M.D. Whale, "A Flucuatational Electrodynamics Analysis of Microscale Radiative Transfer and the Design of Microscale Thermophotovoltaic Devices, PhD Thesis submitted to Massachusetts Institute of Technology (June 1997).

- [13] J.L. Pan, H.K.H. Choy and C.G. Fonstad, *IEEE Trans. Electron. Dev.*, **47**, 241 (2000).
- [14] C.T. Ballinger, G.W. Charache, C.S. Murray, "Monte-Carlo Analysis of Monolithic Interconnected Module with a Back Surface Reflector," *AIP Conf. Proc.* **460**, 161 (1999).
- [15] G.W. Charache et al., *J. Electronic. Mat.*, **27**, 1138 (1998).
- [16] G.W. Charache et al., "InGaAsSb Thermophotovoltaic Diode: Physics Evaluation", *J. Appl. Phys.* **85**, 2247 (1999).
- [17] C. Henry, "Limiting Efficiencies of Ideal Single and Multiple Energy Bandgap Terrestrial Solar Cells," *J. Appl. Phys.*, **51**, 4494 (1980).
- [18] A.L. Fahrenbruch and R.H. Bube, *Fundamentals of Solar Cells*, (Academic Press, New York, 1983).
- [19] C.K. Gethers, C.T. Ballinger, M.A. Postlethwait, D.M. DePoy, and P.F. Baldasaro, "TPV Efficiency Predictions and Measurements for a Closed Cavity Geometry," *AIP Conf. Proc.* **401**, 471 (1997).

List of Figures

Figure 1 - Schematic diagram of major components in a thermophotovoltaic generator concept.

Figure 2 - Comparison of solar versus thermophotovoltaic energy dispersion spectrum.

Figure 3 - Total intensity of energy transfer between hot and cold bodies versus separation for various combinations of materials (■ - semiconductor / semiconductor, □ - metal / semiconductor, Δ - oscillator / oscillator, ◇ - metal / oscillator, ○ - metal / metal) [11].

Figure 4 - Usable (above bandgap) blackbody energy fraction versus bandgap for a 1000 °C radiator.

Figure 5 - Energy diagram representation of thermophotovoltaic energy conversion process.

Figure 6 - TPV performance factor functionality versus diode bandgap assuming a thermodynamically limited dark current ($T_h = 1000$ °C, $T_c = 25$ °C, $\eta_{\text{Carnot}} = 75\%$).

Figure 7 - TPV diode efficiency [EQ(4)] and power density versus diode bandgap assuming perfect filter for two cases: thermodynamically-limited dark current – solid lines, 100x thermodynamically-limited dark current – dashed lines ($T_h = 1000$ °C, $T_c = 25$ °C, $\eta_{\text{Carnot}} = 75\%$).

Figure 8 - TPV efficiency [$\eta = \eta_{\text{diode}} * \eta_{\text{spectral}} = \text{EQ}(4) * \text{EQ}(15)$] versus diode bandgap assuming thermodynamically-limited dark current (i.e., zero defect, photon-recycled) and various below-bandgap filter reflectivities.

Figure 9 - Effect of parasitic cavity absorption on overall TPV efficiency (Inset: schematic diagram of typical TPV cavity).

FIGURE 1

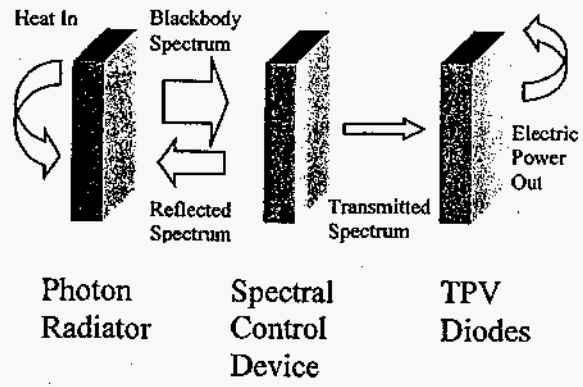


FIGURE 2

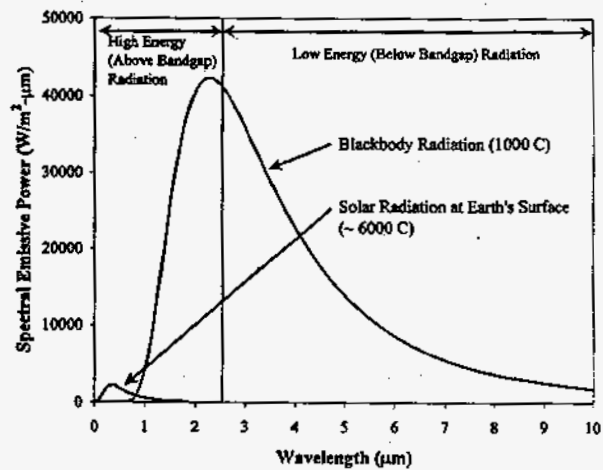


FIGURE 3

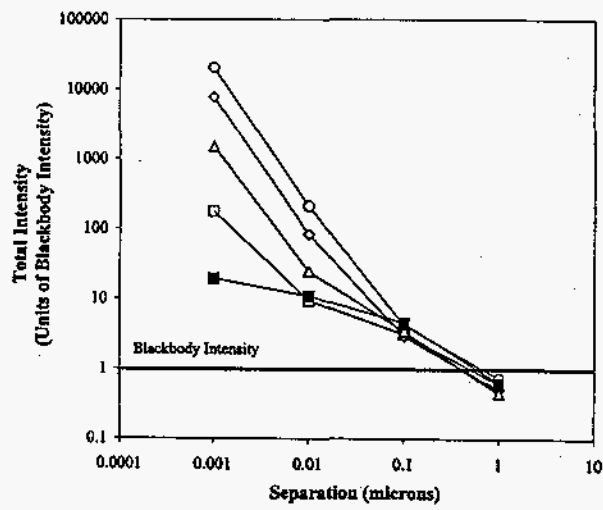


FIGURE 4

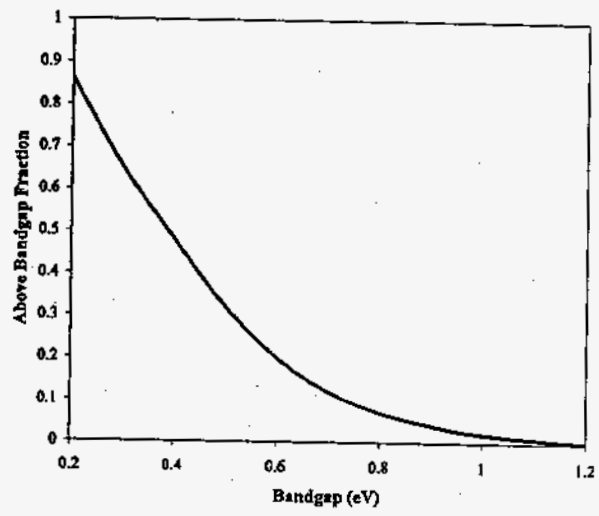


FIGURE 5

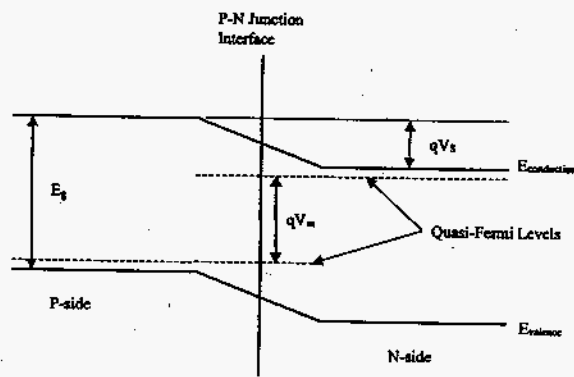


FIGURE 6

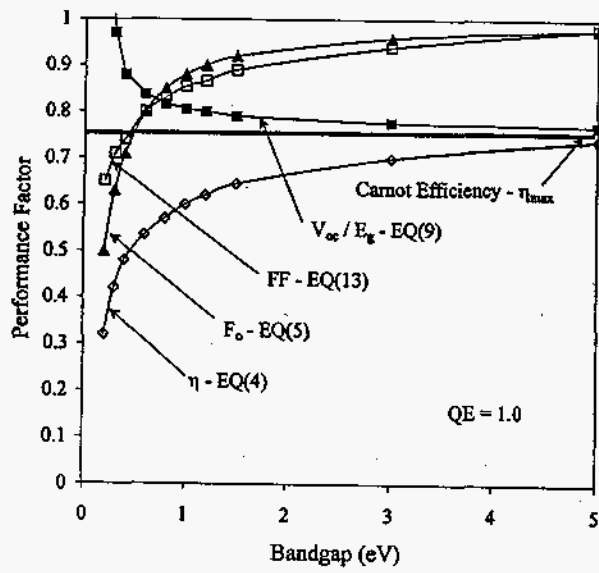


FIGURE 7

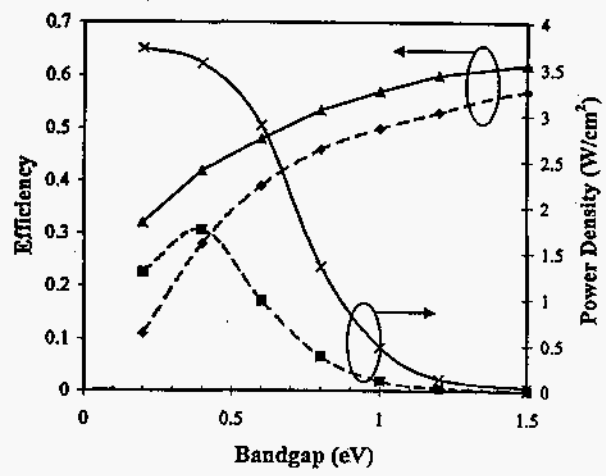


FIGURE 8

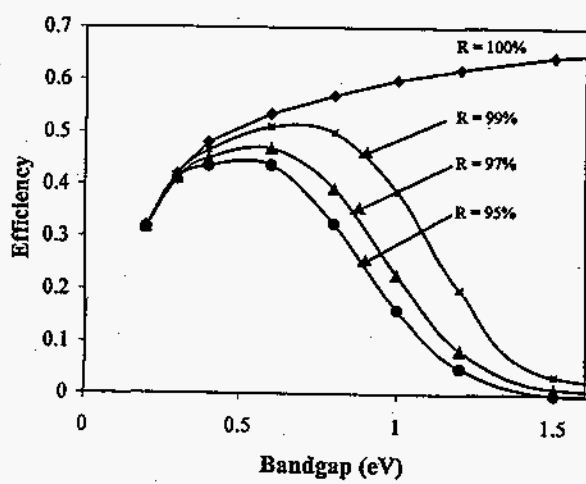


FIGURE 9

